
Article:
Hobbs, M. orcid.org/0000-0003-4661-692X and Willmott, J.R. orcid.org/0000-0002-4242-1204 (2019) InGaAs APD thermometry. Measurement Science and Technology, 31 (1). 014005. ISSN 0957-0233

https://doi.org/10.1088/1361-6501/ab41c6

InGaAs avalanche photodiode thermometry

OPEN ACCESS
IOP Publishing
Measurement Science and Technology
Meas. Sci. Technol. **31** (2020) 014005 (7pp)
https://doi.org/10.1088/1361-6501/ab41c6

InGaAs avalanche photodiode thermometry

Matthew James Hobbs and Jon R Willmott

Department of Electronic and Electrical Engineering, The University of Sheffield, Sheffield S1 4DE, United Kingdom

E-mail: j.r.willmott@sheffield.ac.uk

Received 27 June 2019, revised 2 September 2019
Accepted for publication 5 September 2019
Published 24 October 2019

Abstract

The infrared detector is the most important component within any radiation thermometry-based system, with its choice determining the wavelength, response time and, ultimately, the temperature measurement capabilities of the instrument. To improve upon the existing generation of radiation thermometers, more sensitive detector technologies are required. In this work, we demonstrate a direct comparison between an indium gallium arsenide (InGaAs) photodiode and an InGaAs avalanche photodiode (APD) for 1.6 μm radiation thermometry. The high internal gain of the InGaAs APD increases the sensitivity of the radiation thermometer, enabling the measurement of a target temperature more than 50 °C lower than is typical with commercially available InGaAs photodiode thermometers. The more sensitive InGaAs APD provides faster response time measurements, hence improving the thermometer's temporal resolution. Finally, the InGaAs APD is shown to produce a quantitative thermal image with lower measured temperature fluctuation across the scene when incorporated within a highly aperture limited scanning system.

Keywords: radiation thermometry, InGaAs, avalanche photodiode, temperature measurement

(Some figures may appear in colour only in the online journal)

1. Introduction

Radiation thermometers operating at 1.6 μm are used for general purpose non-contact temperature measurement applications. Commercial instruments typically measure target temperatures down to 300 °C [1, 2], although they can also be used to measure below the indium point of 157 °C under specific configurations [3]. Typical photodetector technologies used within such instruments are germanium (Ge) and indium gallium arsenide (InGaAs) photodiodes [4–7], due to their strong photoresponse at this application wavelength. In recent times, the InGaAs photodiode has overtaken the Ge photodiode as the dominant detector technology for 1.6 μm radiation thermometry due to its higher shunt resistance, lower noise and lower ambient temperature dependence [8].

For optical communication applications, the InGaAs photodiode has itself been largely replaced by the InGaAs avalanche photodiode (APD) [9, 10]. InGaAs APDs take advantage of an internal gain mechanism which increases their sensitivity; therefore, enabling detection of weaker signals and higher speed operation. In optical communications, this translates to higher bit rate data transmission over longer distances. In order to improve upon the current generation of 1.6 μm radiation thermometers, the InGaAs APD is, therefore, suggested as an alternative detector technology. Its increased sensitivity should lead to the measurement of lower target temperatures, improve the signal-to-noise ratio (SNR) of inherently aperture limited instrumentation and enable faster speed measurements. The latter is especially important for the development of instruments capable of measuring fast transitions whilst still maintaining good noise performance within the temperature measurement.

We have previously demonstrated a Si APD for 1 μm radiation thermometry in comparison with a Si photodiode, demonstrating that the Si APD can measure a lower minimum target temperature [11, 12]. It would, therefore, be reasonable to also expect the InGaAs APD to offer improvement in performance over an InGaAs photodiode. In this work, we demonstrate an InGaAs APD as a viable detector technology for non-contact temperature measurement in direct comparison with

an InGaAs photodiode. The more sensitive InGaAs APD is shown to measure a target temperature more than 50 °C lower than an InGaAs photodiode, enable faster speed temperature measurements and produce a quantitative thermal image with lower fluctuation in the measured temperature when operated within a highly aperture limited scanning system.

2. Theory and experimental methods

Internal gain, known as avalanche gain, of APDs is brought about by the impact ionisation process [13]. This occurs when free carriers, either electrons or holes, obtain sufficient energy such that new electron–hole pairs are generated upon the free carriers' collisions with the semiconductor material lattice. When a reverse bias voltage is applied across the APD, the electric field strength is increased, which in turn accelerates the free carriers and leads to a chain of impact ionisation events. The end result is an increase in electron–hole pairs, and thus avalanche gain. The magnitude of this gain within an APD is dependent upon the semiconductor material it is made from, and, more specifically, the ionisation coefficients of that material [14]. These are the average number of ionisation events which occur per unit distance travelled by free carriers within the material. Due to the ionisation coefficients exhibiting a strong electric field dependence, the overall level of APD gain is thus dependent upon the applied reverse bias voltage.

With impact ionisation being stochastic in nature, there is inevitably a fluctuation in the magnitude of the avalanche gain about its mean value. This gives rise to a level of noise, known as excess noise [15]. APDs are only advantageous to optical measurement systems if the noise they introduce is lower than the noise of the amplifier they are used with. This implies that there is an optimum level of gain which the APD needs to operate at for maximum SNR performance [16]. An assessment of this will be performed for our InGaAs APD thermometer to establish its optimum operating condition and for further analysis.

The detectors investigated were the Hamamatsu G11193-02R InGaAs photodiode, and the Hamamatsu G8931-20 InGaAs APD [17, 18]. The experimental setup used for the thermometers is shown in figure 1, designed to reflect a configuration that is typical within commercially available instruments. Each thermometer consisted of the detector soldered upon a printed circuit board (PCB) within a conventional transimpedance amplifier (TIA) circuit configuration. The TIA circuit comprised an OPA657 op-amp and a resistor–capacitor (RC) feedback network of 2 MΩ and 1.8 pF. This was followed by a first order RC filter (1 kΩ and 1 nF) for further filtering, leading to an overall circuit response time of approximately 10 μs. From the detector datasheets, the shunt resistance of the InGaAs photodiode is stated as 1.4 GΩ, whilst that of the InGaAs APD was estimated be of a similar magnitude. The reverse bias voltage for the APD was generated using a Laser Components 550-06 high voltage biasing module. The applied bias voltage was controlled using trimming potentiometers to vary the bias voltage between −20 V and −50 V using the analogue voltage control method outlined in the biasing module datasheet [19]. The noise generated from these bias setting potentiometers under 'worst case' bias conditions was estimated to contribute less than 1 mV to the APD bias voltage. A 2 kΩ temperature sensor was incorporated next to the APD to enable the biasing module to perform ambient temperature correction. The output of the TIA circuit was connected to a National Instruments USB-6212 data acquisition unit (NI-DAQ), which, in turn, was connected to a computer utilising a Labview data logging and processing program.

The PCB was screwed into an optics mount containing a BK7 singlet lens which focused the emitted radiation from the target onto the detector. Variable diameter circular target apertures were placed in front of an AMETEK LAND Landcal P550P blackbody reference furnace, with a manufacturer quoted emissivity of greater than 0.995; this provided a target for the temperature measurements. For calibration purposes, the furnace temperature was measured using an ISOTECH milliK precision thermometer with transfer standard platinum resistance thermometer (PRT).

The active area of both detectors were 0.2 mm in diameter, which served as the thermometer field stops. The field-of-view (FOV) was measured for both thermometers and found to be approximately 100:1, defined at the point at which the FOV contains 90% of the radiant power from the target source based upon a paraxial image of the system field stop. This was equivalent to a FOV of approximately 5 mm in diameter at an operating distance of 500 mm. Subsequent calibration and measurements were, therefore, performed with a twice nominal target aperture of 10 mm in diameter. Glare within the measurement was reduced by positioning a 0.8 mm glare stop directly above the detector active area, whilst an RG850 daylight filter was positioned above this to remove the effect of ambient light. No additional aperture stops were introduced, leading to a system *f*-number of *f*/2.

Calibration of the thermometers used the Wien approximation to Planck's law, which denotes the relationship between a blackbody's radiant exitance as a function of temperature and wavelength, as shown in equation (1). This was valid as the measurements were primarily concerned with wavelengths shorter than the peak in blackbody emission.

$$L(\lambda, T) = \frac{c_1}{\lambda^5} \exp\left(\frac{-c_2}{\lambda T}\right) \tag{1}$$

$$V = \int_{\lambda_1}^{\lambda_2} R(\lambda) \cdot L(\lambda, T) \cdot \mathrm{d}\lambda. \tag{2}$$

The spectral radiance of a perfect blackbody is denoted by L, whilst c_1 and c_2 are the first and second radiation constants, respectively. Target temperature and wavelength are denoted by T and λ, respectively, with T in units of kelvin. The relationship between the output voltage of a radiation thermometer, V, and the target temperature can be plotted as $\ln(V)$ against $1/T$ [20]. The extended effective wavelength, λ_x, can be approximated by taking the gradient of this plot and can be used to characterise the operating wavelength of the thermometer [21, 22]. This plot also enables an assessment of the linearity of the

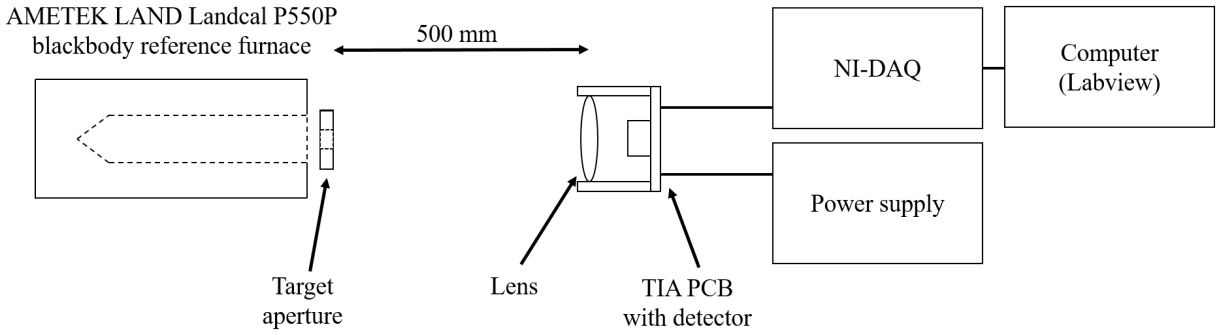

Figure 1. Radiation thermometry measurement setup for InGaAs photodiode and InGaAs APD thermometers.

radiation thermometer as a function of target temperature. The bandwidth for the integral in equation (2), corresponding to the signal voltage, is limited at the short wavelength end, λ_1, by the RG850 filter and at the long wavelength end, λ_2, by the cut-off wavelength of the detector. The spectral responsivity of the filter and detector combination is represented by $R(\lambda)$. Thermometer calibration was performed by use of a standard calibration procedure [12], resulting in a relationship between the output voltage and the target temperature.

A measure of the thermometers' SNR was calculated by dividing the mean by the standard deviation for the output voltage logged every 10 μs over a 10 second period. Various levels of averaging were applied to the measured data to reflect different levels of instrument integration time; this approach effectively increases the SNR at the expense of overall instrument response time. The root-mean-squared (RMS) noise of the thermometers can be calculated by taking the standard deviation value of the calibrated temperature measurement.

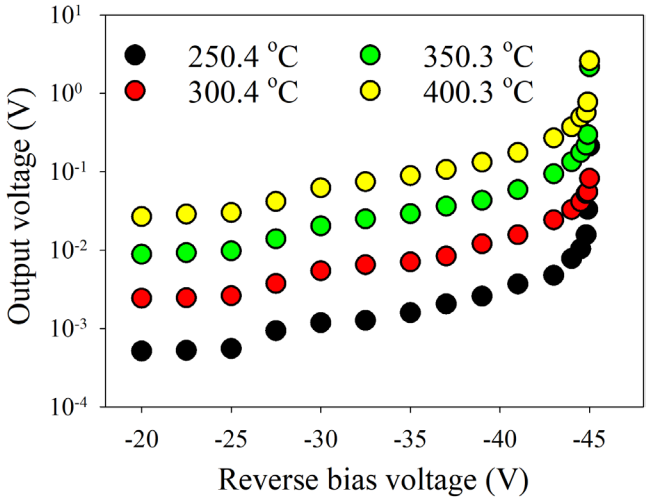

Figure 2. Output voltage of InGaAs APD thermometer as a function of reverse bias voltage for target temperatures of 250.4 °C, 300.4 °C, 350.3 °C and 400.3 °C.

3. Results and discussion

To find the optimum bias voltage for the InGaAs APD thermometer, we measured its output voltage at various set values. This was performed for target temperatures of 250.4 °C, 300.4 °C, 350.3 °C and 400.3 °C, as shown in figure 2. Note, the dark voltage of the thermometer has been subtracted from the displayed value; this is required as part of the calibration procedure.

Increase in output voltage follows increase in reverse bias voltage for the InGaAs APD thermometer. There appears to be three distinct stages within figure 2: −20 V to −25 V; −27.5 V to −44 V; and above −44 V. Between −20 V and −25 V, there is no significant change in the output voltage. The APD is operating within its unity gain region, a region within which the collection of primary photo generated carriers is at its largest whilst impact ionisation has not yet turned on [23]. The APD is operating beyond its punch-through voltage, which is the point at which the depletion region has penetrated the charge layer between absorption and multiplication layers. Increasing the reverse bias voltage to −27.5 V and beyond results in the output voltage increasing at a greater rate; the impact ionisation process is now in effect. This increases further with increased field strength at larger reverse bias voltages. Beyond −44 V, the electric field within the APD has become so large such that avalanche breakdown, the point at which the impact ionisation process becomes significant due to a large increase in free carriers, has begun. The larger field strength leads to a rapid increase in the output voltage caused by the greater magnitude of avalanche gain. It is within this region that excess noise would be expected to be introduced to the measurement, which ultimately becomes detrimental to the overall instrument SNR.

In order to perform a simple analysis to approximately quantify the gain of the APD, the output voltage was normalised to its value at −20 V, a point within the APD's unity gain region. This is shown in figure 3(a). The gain is observed to be roughly consistent across the measured temperature range as a function of bias voltage, indicating that any wavelength dependent gain mechanisms are minimal over this target temperature range. Any slight discrepancies within the gain measurement are believed to be due to a combination of drift in the APD gain with ambient temperature and precision within our bias control method. This issue becomes more noticeable at the highest of reverse bias voltages which correspond to the higher gain values. At such high and rapidly increasing gain values, gain needs increased precision; slight error in the bias voltage leads to a larger error in gain. However, whilst it may seem intuitive to operate the APD at the highest gain possible to enable higher output voltage, this does not consider the

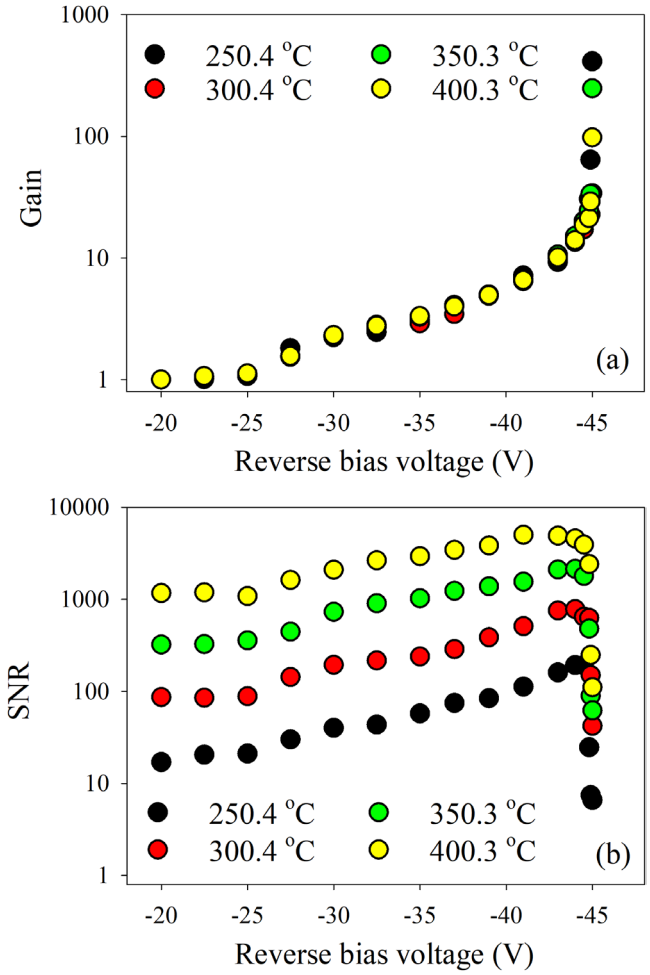

Figure 3. (a) APD gain and (b) SNR with 5 ms integration time for InGaAs APD thermometer as a function of reverse bias voltage for target temperatures of 250.4 °C, 300.4 °C, 350.3 °C and 400.3 °C.

excess noise introduced by the APD and the effect this has on the overall instrument SNR. Figure 3(b) shows the SNR of the InGaAs APD thermometer with an integration time of 5 ms. There is concomitant increase in SNR with APD gain up to a maximum point, after which follows a sharp decrease in SNR. At this point, the excess noise introduced by the APD has become larger than the system noise and, therefore, starts to degrade the measurement SNR. Further increase in reverse bias voltage, and hence excess noise, only serves to compound this issue further. The optimum operational reverse bias voltage for our InGaAs APD thermometer is the point of its maximum SNR; this was found to be −44 V, corresponding to an approximate APD gain of 14. Although operation above this bias voltage would increase the gain, the measurement would become noisy and unstable.

To directly compare the InGaAs APD thermometer against the InGaAs photodiode thermometer, the output voltage as a function of target temperature is shown in figure 4(a), whilst a plot of ln(V) against 1/T is shown in figure 4(b). In addition to operating the InGaAs APD at its optimum bias voltage of −44 V, measurements were repeated at bias voltages of −30 V, −39 V and −44.8 V, for comparison, which correspond to gains of 2, 5 and 25, respectively. In accordance with figure 2,

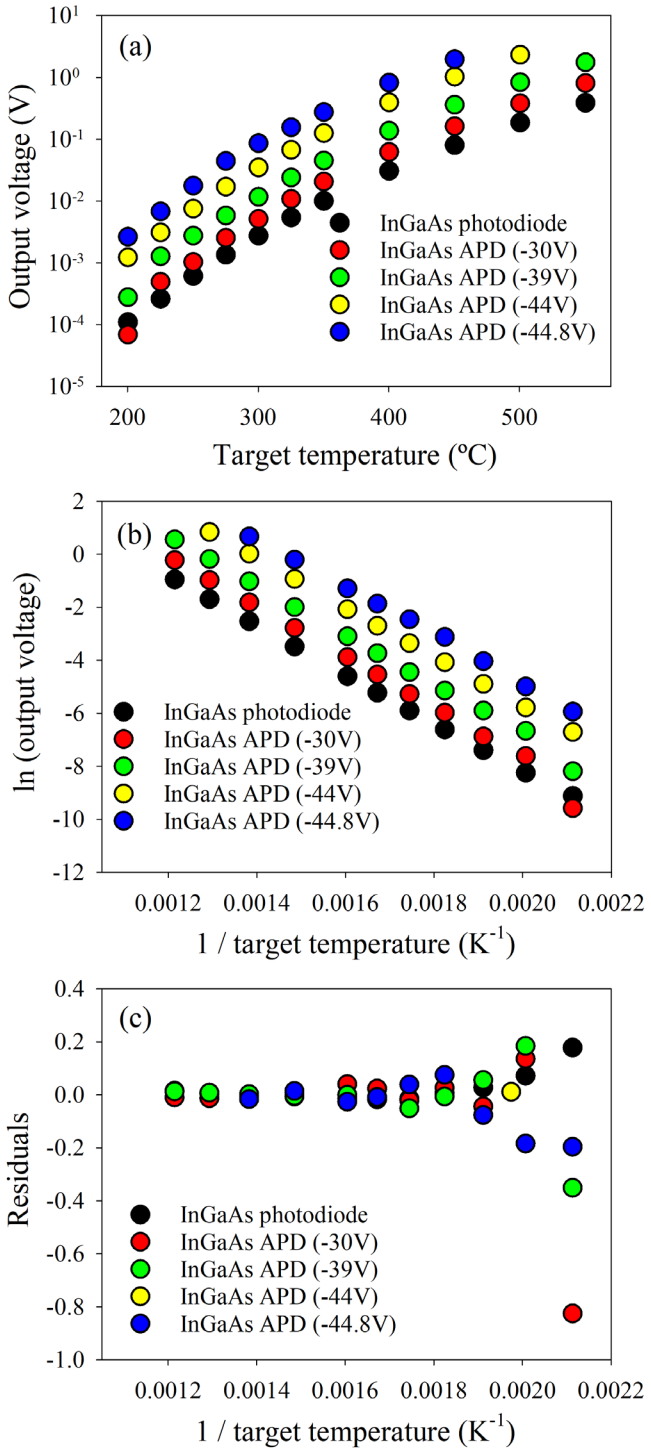

Figure 4. (a) Output voltage of InGaAs photodiode and InGaAs APD thermometers as a function of target temperature and (b) 1/T against ln(V) plot for InGaAs photodiode and InGaAs APD thermometers, with APD reverse bias voltages of −30 V, −39 V, −44 V and −44.8 V. (c) Residuals of the 1/T against ln(V) plot in comparison with the calibration from the Wien approximation.

there is concomitant increase in output voltage with increased reverse bias, whilst all APD thermometer measurements show a higher output voltage over the reverse bias range than the photodiode thermometer. All the APD thermometer measurements appear to obey the Wien approximation to Planck's law. This is confirmed in figure 4(c) which shows the residuals of

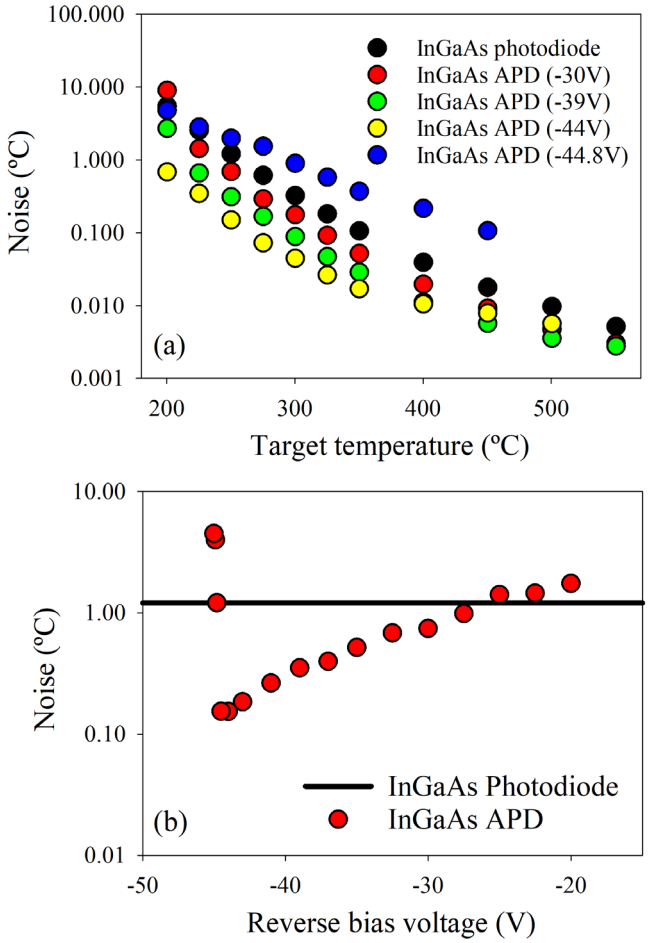

Figure 5. (a) Noise of InGaAs photodiode and InGaAs APD thermometers with target temperature. (b) Noise as a function of InGaAs APD reverse bias voltage for a target temperature of 250.4 °C, compared with the unbiased InGaAs photodiode. Integration time of 5 ms.

the measurement in figure 4(b) in comparison with our calibration from the Wien approximation. The linearity of the $\ln(V)$ against $1/T$ relationship, whilst not essential, eases the calibration process for the InGaAs APD within a radiation thermometer. There is a drop-off in the linearity at the lowest of temperatures for both thermometers, but this should be expected; the signal is at such a low level that it is approaching the instrument noise floor. By measuring the gradients within the linear regions of these plots, λ_x was calculated for each APD bias voltage. Between −30 V and −44 V, λ_x increased from 1.523 μm to 1.540 μm, before a larger increase to 1.649 μm for −44.8 V. This indicates a gain dependence in λ_x which dictates additional calibration would be required if an instrument were to utilise variable APD gain within its operation, accounting for change in both λ_x and signal level. However, if we limit operation only up to the optimum bias voltage of −44 V, the variation in λ_x is relatively small.

The noise within the measurements is shown in figure 5(a), using an instrument integration time of 5 ms. Whilst there is steady reduction in the noise with increased APD bias voltage, there is a clear increase at −44.8 V; the higher thermometer noise corresponds to the lower SNR seen in figure 3(b). This is illustrated in figure 5(b), which shows a direct comparison at a target temperature of 250 °C between the InGaAs photodiode and the InGaAs APD thermometers with different levels of reverse bias voltage. At reverse bias voltages between −20 V and −25 V, the noise of the InGaAs APD measurement is comparable with that of the InGaAs photodiode. However, when impact ionisation turns on from −27.5 V, the noise of the InGaAs APD thermometer drops below that of the InGaAs photodiode thermometer in accordance with its increased gain. The noise continues to fall until a minimum value at the optimum reverse bias voltage of −44 V. When operating beyond this point, there is a sharp increase in noise due to the excess noise of the APD starting to dominate the system noise. For the 250.4 °C target, the InGaAs photodiode thermometer noise is ±1.20 °C, whilst that of the −44 V biased InGaAs APD thermometer is ±0.15 °C. Noise introduced by the bias setting potentiometers was estimated to represent a minimal contribution to the thermometer noise over the measured temperature range.

A typical RMS noise specification of a radiation thermometer is ±0.5 °C [2]. The InGaAs photodiode thermometer, within its typical commercial configuration, achieves this noise specification above 275 °C whilst the InGaAs APD thermometer achieves this same noise specification below 225 °C. This, therefore, represents greater than 50 °C improvement in the minimum temperature that can be measured. This improvement, provided by its internal gain, demonstrates how the APD can measure lower target temperatures without the need for a longer wavelength or larger active area detector.

4. Further implementation

Whilst enabling a 1.6 μm radiation thermometer to measure a lower minimum temperature is clearly advantageous, there are further potential benefits of using a more sensitive detector for radiation thermometry. Such scenarios include measuring temperature with a faster data capture rate and the integration of the InGaAs APD within instrumentation which is inherently aperture limited. We will consider the InGaAs APD for these scenarios here.

Figure 6 shows the noise comparison between the InGaAs photodiode and InGaAs APD thermometers, biased at −44 V, at fixed target temperatures of (a) 250.4 °C and (b) 400.3 °C. The measurement integration time was varied to demonstrate the effect this has upon the noise and, ultimately, the potential operating speed of the instrument whilst still maintaining reasonable noise performance. Again taking a ±0.5 °C noise specification, the InGaAs photodiode and InGaAs APD thermometers require integration times of approximately 100 ms and 100 μs, respectively, for the measurement of the 250.4 °C target. For the 400.3 °C target, the same ±0.5 °C noise specification is met at an integration time of approximately 10 μs for the InGaAs photodiode thermometer. We were unable to measure the InGaAs APD thermometer integration time for a ±0.5 °C noise measurement, due to the DAQ unit's maximum acquisition speed of 10 μs. However, with faster readout electronics, we would clearly be able to perform a faster measurement than is capable with the InGaAs photodiode thermometer for such a scenario.

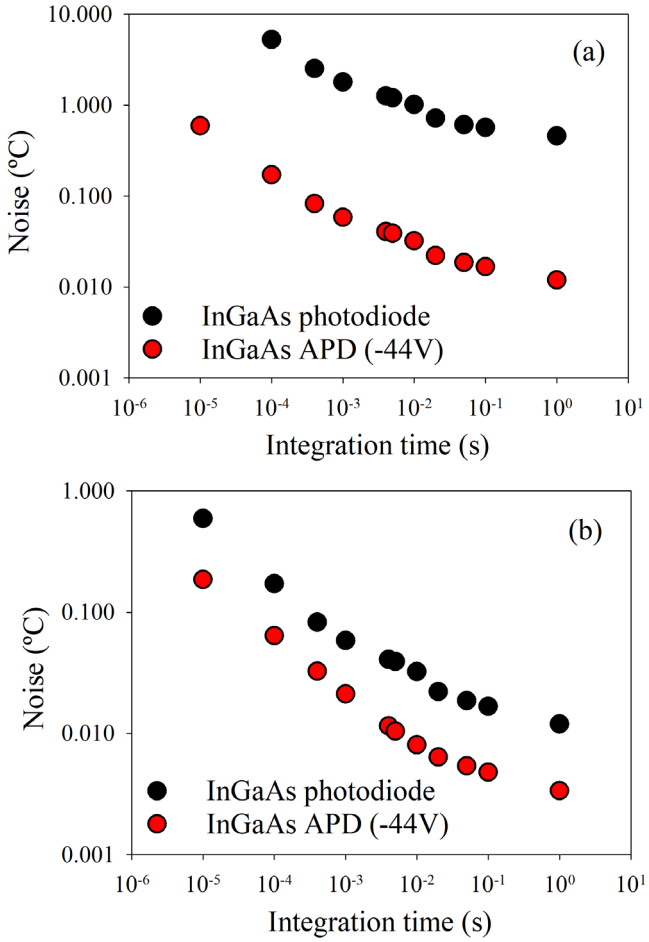

Figure 6. Noise of InGaAs photodiode and InGaAs APD thermometers as functions of integration time. Target temperatures of (a) 250.4 °C and (b) 400.3 °C.

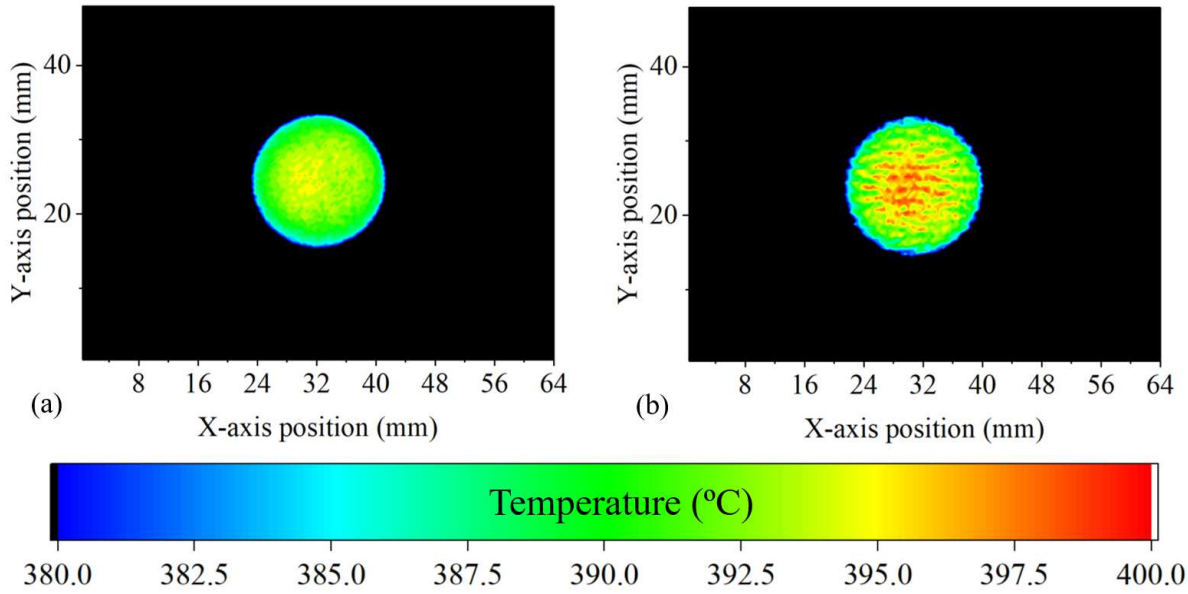

Figure 7. Thermal images of a 20 mm diameter target aperture placed in front of a furnace at a temperature of 395 °C, using (a) InGaAs APD and (b) InGaAs photodiode-based scanners.

To demonstrate the benefit of the InGaAs APD for use within aperture limited instrumentation, we integrated the InGaAs APD, with its PCB, glare stop and filter, into a micro-electro-mechanical systems (MEMS) mirror scanning system. This was tested under the same configuration and test setup described in [24], with the measurements repeated for the InGaAs photodiode. Given a system *f*-number of *f*/16, significantly less signal reaches the detector compared to our *f*/2 radiation thermometer. Therefore, the increased sensitivity provided by the InGaAs APD can help compensate for this. Figure 7 shows thermal

images of a 20 mm diameter aperture placed in front of a furnace at a temperature of 395 °C for both the (a) InGaAs APD and (b) InGaAs photodiode-based scanners.

Observing the two images, it is clear that there is reduced noise within the InGaAs APD image compared to that within the InGaAs photodiode image, thus in agreement with our earlier results. The approximate fluctuation in the measured temperature within the images are ±1 °C and ±3 °C for the InGaAs APD and InGaAs photodiode-based scanners, respectively. In addition to further showcasing the advantage provided by the more sensitive InGaAs APD, this also demonstrates, to the best of our knowledge, the first example of an InGaAs APD used for thermal imaging with a quantitative temperature measurement.

5. Conclusion

We have demonstrated an InGaAs APD to be a more sensitive detector technology for use within 1.6 μm radiation thermometry-based instrumentation. In direct comparison with an InGaAs photodiode, the high internal gain of the InGaAs APD resulted in a higher voltage upon the thermometer's output. Whilst operating at its optimum gain of 14, the InGaAs APD was shown to offer more than 50 °C improvement in the minimum measurable temperature for a specified thermometer noise. The InGaAs APD thermometer exhibited a gain dependence in λ_x, although this was found to be small if operation was limited only up until its optimum gain value. The increased sensitivity of the InGaAs APD enabled us to demonstrate faster speed measurement acquisition in comparison with the InGaAs photodiode. Finally, we integrated the InGaAs APD within a highly aperture limited scanning system. This was demonstrated to produce a thermal image with less fluctuation in the measured temperature across the scene compared to the equivalent for an InGaAs photodiode.

Acknowledgments

This work has been supported by Engineering and Physical Sciences Research Council (EPSRC) fellowship EP/M009106/1.

ORCID iDs

Matthew James Hobbs https://orcid.org/0000-0003-4661-692X
Jon R Willmott https://orcid.org/0000-0002-4242-1204

References

[1] Dixon J 1988 Radiation thermometry *J. Phys. E Sci. Instrum.* **21** 425–36
[2] Land Instruments International 2018 SPOT-High Precision Pyrometers (https://www.ametek-land.com/-/media/ameteklandinstruments/documentation/products/fixedspotnoncontactthermometers/spot/ametek_land_spot_brochure_rev_18_en.pdf) (Accessed: 13 September 2019)
[3] Sakuma F, Ma L and Kobayashi T 2008 Development of a new InGaAs radiation thermometer at NMIJ *Int. J. Thermophys.* **29** 312–21
[4] Beynon T G R 1981 Turbine pyrometry: an equipment manufacturer's view *ASME Gas Turbine Conf. and Products Show (Houston, USA, March 1981)* ASME 81-GT-136
[5] Tapia G and Elwany A 2014 A review on process monitoring and control in metal-based additive manufacturing *Trans. ASME J. Manuf. Sci. Eng.* **136** 060801
[6] Mantilla J, Martin M, Campos J, Hernanz M and del Campo D 2018 Testing irradiance and radiance methods for absolute radiation thermometry based on InGaAs detectors in the NIR at CEM/CSIC *J. Phys.: Conf. Ser.* **1065** 122005
[7] Yoon H, Woodward J, McEvoy H and Machin G 2018 Thermodynamic measurements of Zn and Al freezing temperatures using an InGaAs-based, near-infrared radiation thermometer 3 (NIRT3) *J. Phys.: Conf. Ser.* **1065** 122023
[8] Eppeldauer G P 1997 Electronic characteristics of Ge and InGaAs radiometers *Proc. SPIE* **3061** 833–9
[9] Campbell J C 2007 Recent advances in telecommunications avalanche photodiodes *J. Lightwave Technol.* **25** 109–21
[10] Achouche M, Glastre G, Caillaud C, Lahrichi M, Chtioui M and Carpentier D 2010 InGaAs communication photodiodes: from low-to high-power-level designs *IEEE Photonics J.* **2** 460–8
[11] Hobbs M, Tan C and Willmott J 2013 Evaluation of phase sensitive detection method and Si avalanche photodiode for radiation thermometry *J. Instrum.* **8** P03016
[12] Hobbs M J, Grainger M P, Zhu C, Tan C H and Willmott J R 2018 Quantitative thermal imaging using single-pixel Si APD and MEMS mirror *Opt. Express* **26** 3188–98
[13] Capasso F 1985 Physics of avalanche photodiodes *Semiconductors and Semimetals: Lightwave Communications Technology* (Orlando, FL: Academic) vol 22 pp 1–172
[14] David J and Tan C 2008 Material considerations for avalanche photodiodes *IEEE J. Sel. Top. Quantum Electron.* **14** 998–1009
[15] McIntyre R 1966 Multiplication noise in uniform avalanche diodes *IEEE Trans. Electron Devices* **ED-13** 164–8
[16] Forrest S 1985 Sensitivity of avalanche photodetector receivers for high-bit-rate long-wavelength optical communication systems *Semiconductors and Semimetals: Lightwave Communications Technology* (Orlando, FL: Academic) vol 22 pp 329–87
[17] Hamamatsu Photonics 2017 InGaAs PIN Photodiodes-G11193 Series (https://www.hamamatsu.com/resources/pdf/ssd/g11193_series_kird1111e.pdf) (Accessed: 13 September 2019)
[18] Hamamatsu Photonics 2017 InGaAs APD-G8931 Series (https://www.hamamatsu.com/resources/pdf/ssd/g8931_series_kapd1018e.pdf) (Accessed: 13 September 2019)
[19] Laser Components 2015 Mini High Voltage Modules ABC 550-Series (https://www.lasercomponents.com/fileadmin/user_upload/home/Datasheets/lce/abc-550-series.pdf) (Accessed: 13 September 2019)
[20] Hahn J and Rhee C 1994 Interpolation equation for the calibration of infrared pyrometers *Metrologia* **31** 27
[21] Bezemer J 1974 Spectral sensitivity corrections for optical standard pyrometers *Metrologia* **10** 47
[22] Saunders P 2003 Uncertainty arising from the use of the mean effective wavelength in realizing ITS-90 *AIP Conf. Proc.* **684** 639–44
[23] Williams G M, Compton M, Ramirez D A, Hayat M M and Huntington A S 2013 Multi-gain-stage InGaAs avalanche photodiode with enhanced gain and reduced excess noise *IEEE J. Electron Devices Soc.* **1** 54–65
[24] Hobbs M J, Zhu C, Grainger M P, Tan C H and Willmott J R 2018 Quantitative traceable temperature measurement using novel thermal imaging camera *Opt. Express* **26** 24904–16